American Journal of Energy Research, 2023, Vol. 11, No. 3, 108-116
Available online at http://pubs.sciepub.com/ajer/11/3/2
Published by Science and Education Publishing
DOI:10.12691/ajer-11-3-2

Comparison of Power Extraction of Wave Energy Converter with Conical and Hemispherical Buoys in the Chengshantou Area

Geng Yuanbo[1], Hassan Ghassemi[1,2,*], Guanghua He[1], Hamid Reza Ghafari[2]

[1]International School of Ocean Science and Engineering, Harbin Institute of Technology, Weihai, China
[2]Marine and Hydrokinetic Energy Group, Department of Maritime Engineering, Amirkabir University of Technology, Tehran, Iran
*Corresponding author: hmaaa2002@gmail.com

Received May 15, 2023; Revised June 24, 2023; Accepted July 2, 2023

Abstract Ocean waves are considered a potentially untapped renewable resource that is 800 times denser than wind energy. With a vast coastline of nearly 32,000 km, China offers a huge potential for harnessing wave energy. This paper utilizes the boundary element method to compare the energy absorption characteristics of two wave energy converters (WECs) with conical and hemispherical buoy shapes (with the same displacement, equal 905203 kg) as point absorber devices in the Chengshantou area of the Shandong Peninsula, which occurs mainly in low and moderate sea states, where a linear response is appropriate. Only heaving motion and regular waves are considered in the hydrodynamic response analysis. Hydrodynamic coefficients such as the Froude-Krylov force, radiation damping, additional mass, diffraction force, excitation force and response amplitude operators (RAO) are compared to determine the most appropriate shape. The maximum efficiency of a power take-off (PTO) device was simulated and the velocity response of the buoy was observed. Monthly variations in average absorbed power and efficiency were calculated for both shapes of the buoy. The results indicate that the hemispherical buoy is more efficient than the conical buoy, due to its better hydrodynamic characteristics and smoother interaction with incident waves.

Keywords: *Shandong peninsula, point absorber, boundary element method, wave energy converter, absorbed power*

Cite This Article: Geng Yuanbo, Hassan Ghassemi, Guanghua He, and Hamid Reza Ghafari, "Comparison of Power Extraction of Wave Energy Converter with Conical and Hemispherical Buoys in the Chengshantou Area." *American Journal of Energy Research*, vol. 11, no. 3 (2023): 108-116. doi: 10.12691/ajer-11-3-2.

1. Introduction

The escalating global energy consumption and conventional approaches to energy generation have resulted in significant ecological challenges. Renewable energy sources could serve as a crucial solution to fulfill the increasing energy demands. Solar power, wind energy, and oceanic resources (such as waves, tides, and currents) emerge as viable alternatives to fossil fuels [1]. Among the innovative renewable energy options, wave energy stands out as a highly promising marine source [2]. Wave energy is recognized as a substantial renewable energy reservoir, with minimal adverse environmental effects, necessitating the consideration of economic factors regarding wave energy resource characteristics prior to its implementation.

Typically, economic considerations drive the selection of sites for wave farms, taking into account variations in resources and costs associated with wave energy converters (WECs) and submarine connections to the grid. The technologies for converting wave energy into electricity are still undergoing development [3]. Each technology exhibits different efficiencies based on varying sea conditions. It is widely recognized that the wave energy resource's characteristics, specifically wave parameters, play a crucial role in determining the most suitable WECs for a particular area and optimizing their design parameters [4]. Prior to WEC installation, a comprehensive investigation and characterization of the wave energy resource in terms of wave parameters is necessary. Consequently, several researchers have reported on wave energy resources in different regions of the world. These prior studies have significantly contributed to understanding the wave energy characteristics in various zones globally.

Comprehensive work was carried out on the Wavestar or torus shape WEC with multi-point-absorber around the fixed and floating wind turbine platform by numerical approaches [5,6,7,8,9].

China possesses an extensive coastline and expansive sea areas that harbor abundant oceanic resources. It is estimated that the coastal waters of the Bohai Sea, the Yellow Sea, the East China Sea, and the South China Sea in China contain approximately 12.85 GW of wave power. The average wave power in the coastal waters of certain provinces is illustrated in Figure 1. Considering the wave

energy density and the minimal potential impact on the environment, priority should be given to the development of wave energy resources in the coastal waters of Zhejiang and Fujian provinces. Subsequently, the eastern region of Guangdong Province's coastal waters, the Yangtze Estuary, and the Shandong Peninsula can be considered for further development in wave energy resources [10].

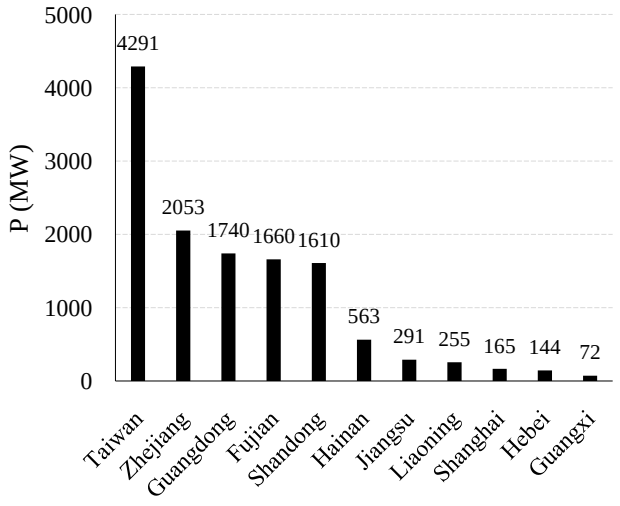

Figure 1. Theoretical power of wave energy in the top 11 provinces in China

Regarding the East China Sea as a whole, the waters near Zhejiang and Fujian exhibit relatively high wave energy density, making them valuable for development and utilization. However, it is important to take into account the region's high frequency of typhoons. The installation and selection of wave energy development equipment should carefully consider the potentially destructive effects of typhoons and large waves. Safeguarding against these factors is crucial for ensuring the successful implementation of wave energy projects in this area.

In conclusion, the wave energy in Shandong province has great potential for development. The objective of this article is to compare the power extraction capabilities of two different buoy shapes in the Chengshantou area, utilizing hydrodynamic coefficients. Additionally, the article aims to predict the monthly variations in mean absorbed power.

2. Theory Description

2.1. Ocean Energy

The sun's thermal radiation is absorbed by the Earth's surface, leading to a temperature differential those results in wind flow from areas of high pressure to low pressure. This wind blowing over the oceans, driven by the Earth's gravity, exerts a frictional force on the ocean's surface, giving rise to the generation of sinusoidal waves. The global wave power is estimated to be approximately 2 TW (terawatts), of which it is believed that around 4.6% of this power can be extracted [11].

Ocean energy may define in terms of energy density per unit width (J) for regular waves using equation (1). Additionally, the maximum power (P_{max}) that can be absorbed by a WEC can be described using equations (2) and (3), with the assistance of the maximum absorption width ($L_{\max}$).

$$J = \frac{\rho g^2}{32\pi} T_e H_s^{\,2} \tag{1}$$

$$L_{\max} = \frac{\lambda}{2\pi} \tag{2}$$

$$P_{\max} = J \cdot L_{\max} \tag{3}$$

where ρ represents the mass density of seawater (1025 kg/m^3), g denotes the gravitational acceleration, T_e represents the wave period, and H_s refers to the significant wave height. The wavelength (λ), for deep-water conditions, can be expressed using equation (4) [12].

$$\lambda = \frac{g}{2\pi} T_e^{\,2} \tag{4}$$

2.2. Linear Wave Theory

A commonly used model for wave energy analysis is the potential flow theory, which makes several assumptions. It assumes that the fluid flow is irrotational, meaning there are no swirls or vortices present. It also assumes the fluid is incompressible and inviscid. Under these assumptions, the linear wave is expressed using the following equation:

$$\eta(t) = A\cos(\omega t + kx) \tag{5}$$

where ω is the frequency in rad/s and k is the wave number.

2.3. Forces on Buoys

To determine the potential power output of a wave energy device, it is necessary to consider a buoy. The governing equation of the buoy in the time domain is defined as follows:

$$M\ddot{z}(t) = F(t) \tag{6}$$

where M represents the mass of the buoy, z denotes the vertical displacement of the buoy, and $F(t)$ represents the total forces acting on the buoy. These forces are classified into two types: viscous forces and non-viscous forces. Viscous forces include form drag and friction drag. The shape of the object influences form drag, with a larger cross-section resulting in higher drag compared to a smaller cross-section. Friction drag arises due to the viscous resistance within the boundary layer surrounding the object. However, in many cases, viscous forces, including friction drag, are relatively small and can be neglected or approximated by using a Morrison force term. In this study, we will not delve into the details of viscous forces.

The buoy experiences hydrodynamic forces in the linear formulation, which encompass the Froude-Krylov force, the diffraction force on a stationary body, and the superposition of the radiation force resulting from the body's motion. These forces are derived from the

principles of potential flow wave theory. In regular waves, the total non-viscous forces on a fixed floating body comprise the combined effects of diffraction and Froude-Krylov forces. The Froude-Krylov force, solely induced by the incident waves, does not account for the body's presence. The pressure on a virtual fixed body in undisturbed waves determines it. The diffraction force arises from the scattering phenomenon involving a combination of wave reflection and diffraction.

$$F_e(\omega) = F_{FK}(\omega) + F_d(\omega) \tag{7}$$

where F_e represents the excitation force, F_{FK} represents the Froude-Krylov force, and F_d represents the diffraction force. According to this theory, it is assumed that the body's dimensions are significantly larger compared to the wavelength of the incoming wave. This assumption ensures that the incoming waves are diffracted by the presence of the buoy. The interpretation of the Froude-Krylov force, stating that the pressure field of the wave is unaffected by the buoy presence, is purely for convenience and is a consequence of linearization. The key aspect enforced by this interpretation is that there is no flow through the fixed rigid body.

The radiation force resulting from the motion of the buoy may be separated into two components: an added mass term and a radiation damping term, as shown in equation (8). This hydrodynamic force arises from the oscillation of the buoy, which, in turn, generates waves. The "added mass" force component is in phase with the buoy motion, while the "radiation damping" term is out of phase with the buoy motion.

$$F_r(\omega) = -\left(-\omega^2 M_a(\omega) + j\omega C(\omega)\right) Z(\omega) \tag{8}$$

where $M_a(\omega)$ is the added mass, $C(\omega)$ is the radiation damping, and $Z(\omega)$ is the heave displacement and j is the imaginary unit.

The added mass is an additional inertia experienced by the buoy undergoing harmonic oscillation due to the presence of the surrounding fluid. It is increased in the effective mass of the buoy.

On the other hand, the radiation damping arises from the motion of the buoy in a fluid, causing outgoing waves that carry energy to infinity. This term is in phase with the buoy velocity and acts as a damping force that is proportional to the velocity of the buoy.

The hydrostatic restoring force, also known as the buoyancy force, aims to restore the buoy to hydrostatic equilibrium. This force arises from the static pressure term, as the wet surface of the buoy is subjected to varying hydrostatic pressures due to its oscillations.

The hydrostatic stiffness (K) is defined as follows:

$$K = \rho g A_w \tag{9}$$

where ρ is the density of the water, g is the acceleration of gravity, and A_w is the waterplane area. This leads to the definition of the hydrostatic force defined as

$$F_{hs}(\omega) = -KZ(\omega) \tag{10}$$

2.4. RAOs

Response Amplitude Operators (RAOs) are transfer functions that quantify the impact of a specific sea state on a buoy immersed in water. The RAOs serve as important tools in assessing the structural response and performance under varying sea states, aiding in the design and optimization of wave energy converters and other marine buoys. They provide valuable insights into the behavior of the buoy and can be used to identify the frequencies at which the maximum amount of power can potentially be extracted.

To calculate the RAO for a particular buoy, a general equation of motion is established. This equation describes the dynamic response of the buoy to the forces acting upon it in the presence of waves. By solving this equation, the RAOs can be obtained, which represent the amplitude and phase relationship between the applied forces and the resulting response of the buoy at different frequencies.

$$-\omega^2 MZ(\omega) = F_e(\omega) + F_r(\omega) + F_{hs}(\omega) \tag{11}$$

where M represents the mass of the buoy. $F_r(\omega)$ denotes the radiation force, $F_{hs}(\omega)$ represents the hydrostatic force, and $F_e(\omega)$ corresponds to the excitation wave force, which includes both incident and diffracting forces.

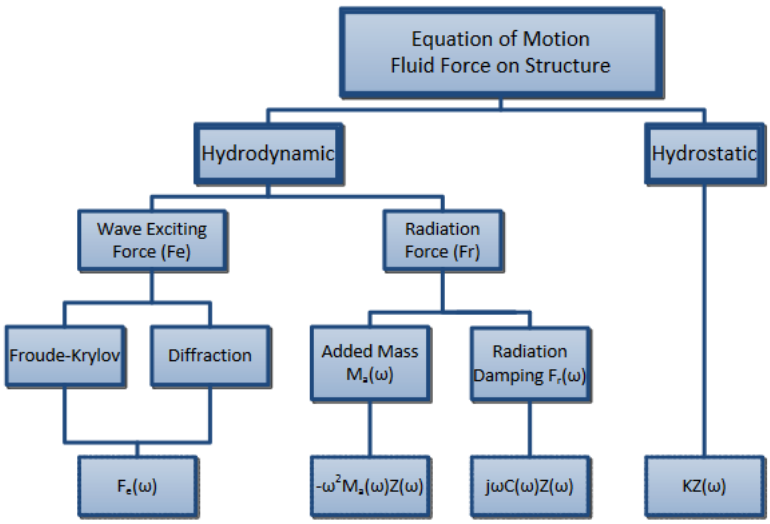

Figure 2. Equation of motion terms of fluid forces acted on a buoy

Figure 2 illustrates the relationship between these terms in equation (11). By solving this equation, we can determine the RAO, which provides the amplitude and phase relationship between the applied forces and the resulting heave response of the buoy at different frequencies.

$$RAO(\omega) = \frac{F_e(\omega)}{K - \omega^2 (M + M_a(\omega)) + j\omega C(\omega)} \quad (12)$$

The RAO is typically represented as a complex quantity, and it is common practice to define the RAO as the magnitude of equation (12) when the phase difference between the incident wave and the motion of the device is not of primary interest. This magnitude-only representation simplifies the analysis and provides a measure of the amplification or attenuation of the response amplitude.

However, it's worth noting that the phase can be significant when optimizing power output. In particular, a 180-degree phase shift between the velocity of the float and the spar can maximize the speed of the generator. Therefore, in certain cases, considering the phase information becomes crucial for achieving the highest possible power output from the WEC [13].

2.5. Mathematical Modelling of PAWEC

The form of WEC considered here is a PAWEC (Point Absorber Wave Energy Converter). According to linear potential theory, the effects of compressibility and viscosity in the flow are disregarded. In the case of a point absorber, it is assumed that the motion occurs solely in the vertical direction (z-direction). The response of a heaving point absorber can be compared to that of a mass-spring system.

By applying Newton's second law of motion, the equation of motion for the point absorber can be represented by equations (13) and (14).

$$\sum_{j=1}^{6}\left(M_{ij} + \alpha_{ij}\right)\ddot{x}_j + \sum_{j=1}^{6}\left(\beta_{ij}\right)\dot{x}_j + \sum_{j=1}^{6}\left(\gamma_{ij}\right)x_j = F_i; \quad i = 1,2,3\ldots,6 \quad (13)$$

For heave motion:

$$\left(M + \alpha_{33}\right)\ddot{x}_3 + \beta_{33}\dot{x}_3 + \gamma_{33}x_3 = F_3 \quad (14)$$

where M_{ij} is the mass of the buoy, α_{ij} is the added mass matrix, β_{ij} is damping matrix, γ_{ij} is hydrostatic stiffness, F_i is the external force in i^{th} mode, $\ddot{x}_j$ is acceleration matrix, $\dot{x}_j$ is velocity matrix and x_j is displacement matrix.

The PTO system is the mechanical component responsible for extracting the kinetic energy from the float's translational motion and converting it into electrical energy through a linear electric generator. The PTO exerts a damping force (F_{PTO}) that opposes the motion of the float. In this case, it is assumed that a simple pure damping motion is achieved, which means that the damping force is frequency-independent [14]. The force applied by the PTO in the heave direction can be represented by equations (15) and (16).

$$\left(M + \alpha_{33}\right)\ddot{x}_3 + \beta_{33}\dot{x}_3 + \gamma_{33}x_3 = F_3 + \delta_{PTO}\dot{x}_3 \quad (15)$$

$$F_{PTO} = \delta_{PTO}\dot{x}_3 \quad (16)$$

where δ_{PTO} is the PTO damping coefficient (N/(m/s)).

In the study conducted by Cargo et al. [15], they proposed optimal conditions for optimizing energy conversion in wave energy systems. One of the key factors they considered was the optimal PTO damping, denoted as $\delta_{PTO(op)}$. The optimal PTO damping is determined by:

$$\delta_{PTO(opt)} = \sqrt{\left(\beta_{33}{}^2 + \left(\omega\left(m + \alpha_{33} - \frac{\gamma_{33}}{\omega}\right)^2\right)\right)} \quad (17)$$

Finally, the absorbed power by the PTO is obtained as follows [16]:

$$P_{PTO} = \frac{1}{2}\delta_{PTO}\omega^2\left|\dot{x}_3\right|^2 \quad (18)$$

3. Results and Discussions

The monthly wave data in 2012 for the Chengshantou area [17] are listed in Table 1. The maximum wave power is shown in December and the minimum is in July. In addition, the wave period of the Chengshantou area fluctuates between 6 and 7s.

Two different buoys are selected for this area (conical and hemisphere). The parameters of different shapes of buoys are listed in Table 2. Figure 3 shows the diffraction panel on the conical and hemisphere buoy's surface.

Table 1. Wave data for Chengshantou area in the year 2012

Month	H_s(m)	T_p(s)	λ(m)	L_{max}(m)	J(kW/m)	P_{max}(kW)
January	3.1	6.52	66.3	10.6	61.4	648.4
February	3.1	6.41	64.1	10.2	60.4	616.2
March	2.4	6.80	72.2	11.5	38.4	440.9
April	1.9	6.92	74.7	11.9	24.5	291.2
May	1.6	6.74	70.9	11.3	16.9	190.8
June	1.5	6.58	67.6	10.8	14.5	156.0
July	1.1	6.45	64.9	10.3	7.6	79.0
August	1.5	6.90	74.3	11.8	15.2	179.9
September	2.2	6.83	72.8	11.6	32.4	375.4
October	2.4	6.51	66.1	10.5	36.7	386.9
November	2.6	6.75	71.1	11.3	44.7	506.1
December	3.3	6.29	61.7	9.8	67.1	659.8

Table 2. Main properties of conical and hemisphere buoys

Parameter	Conical	Hemispherical
Diameter (m)	15	15
Displacement or mass (kg)	905203	905203
Draft (m)	15.375	7.5
COG at z=0 (m)	-3.36	-2.81
$I_{xx}\,(kg.m^2)$	715376	1289119
$I_{yy}\,(kg.m^2)$	715376	1289119
$I_{zz}\,(kg.m^2)$	1252958	1988039

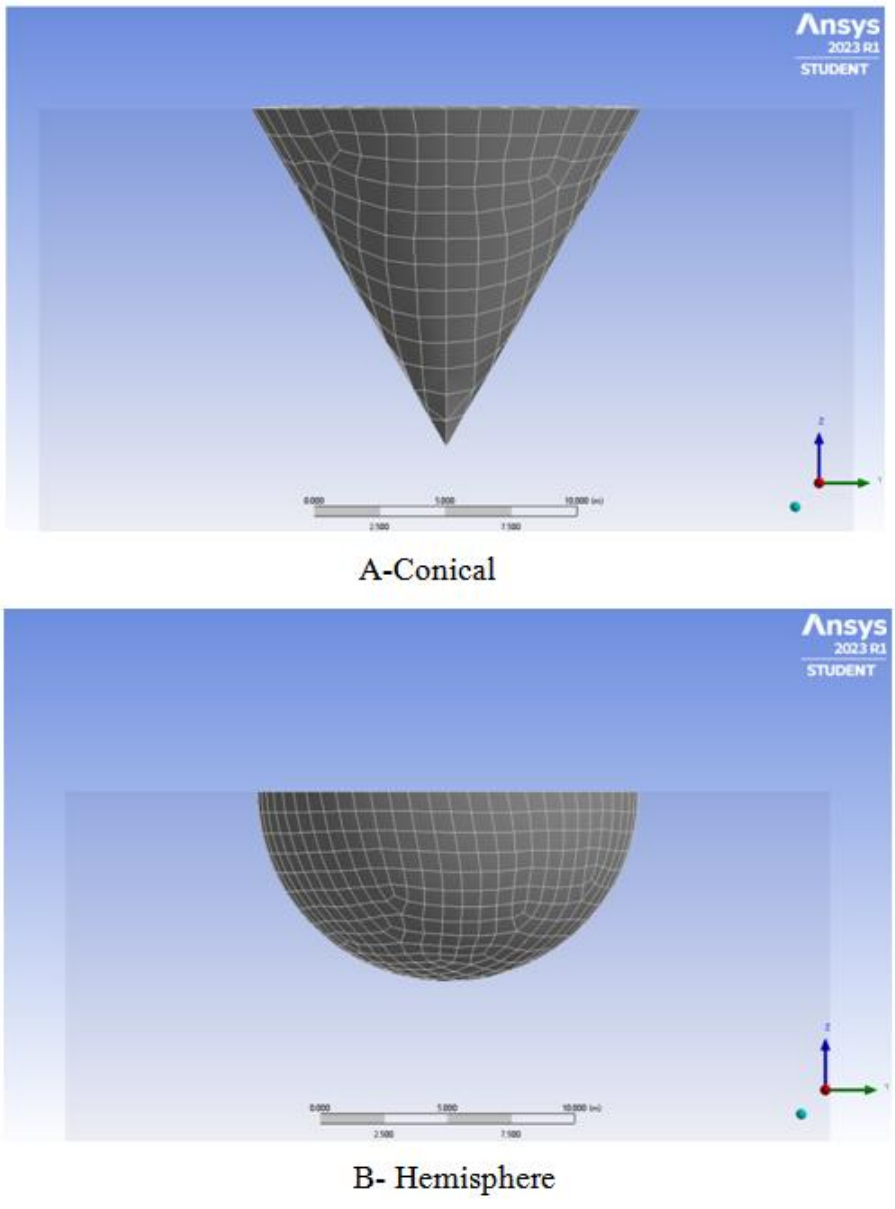

Figure 3. diffraction panel on the conical and hemisphere buoy's surface

The excitation, diffraction and Froude-Krylov forces acted on the conical and hemisphere buoys vs. wave frequencies are shown in Figures 4~6. As can be seen in those figures, for all wave frequencies, excitation and Froude-Krylov for hemisphere are bigger than the conical buoy. Furthermore, these forces are diminished when wave frequency increases. While the trend of diffraction is different for both buoys. Added mass is also shown in Figure 7 for both buoys. Hemisphere added mass is found more than conical buoy, which is reasonable.

In Figure 8 and Figure 9, the radiation damping and RAO of the buoys are shown for the heave motion versus the dimensionless parameter of wave frequency ω^*, which is defined as $\omega^* = \omega\sqrt{\frac{D}{g}}$, where D is the diameter of the buoy. It is observed that the results of the present method are similar to the results of Berenjkoob et al. [18].

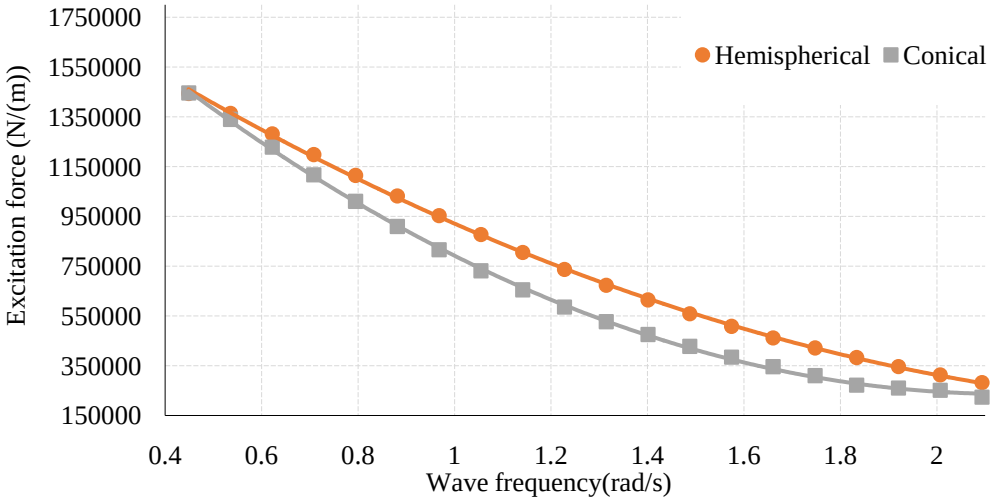

Figure 4. Excitations force vs. wave frequency for conical and hemisphere buoys

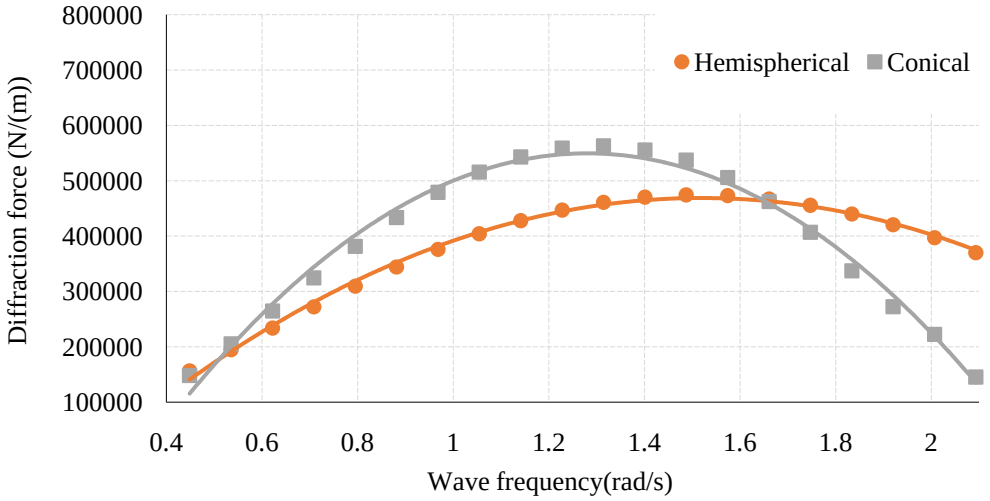

Figure 5. Diffraction force vs. wave frequency for conical and hemisphere buoys

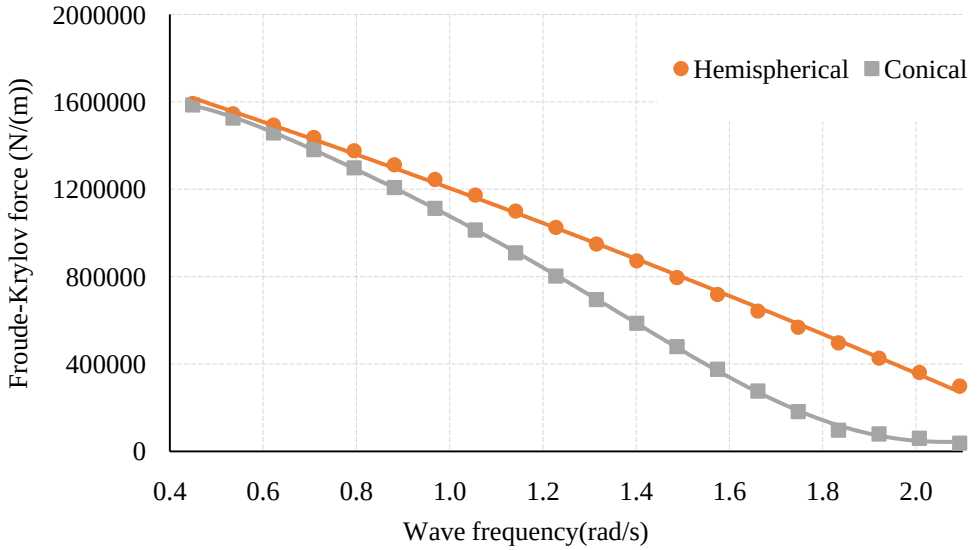

Figure 6. Froude-Krylov force vs. wave frequency for conical and hemisphere buoys

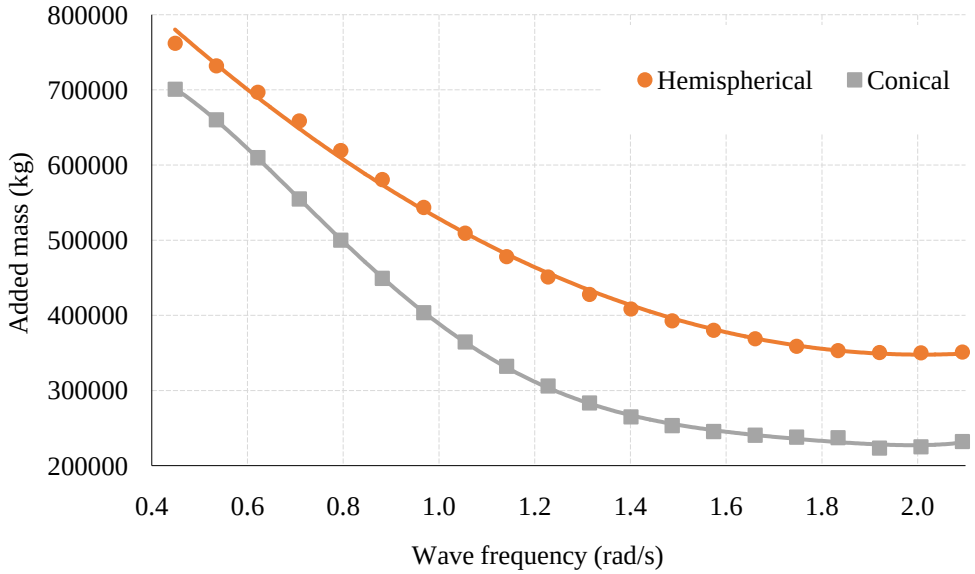

Figure 7. Added mass vs. wave frequency for conical and hemisphere buoys

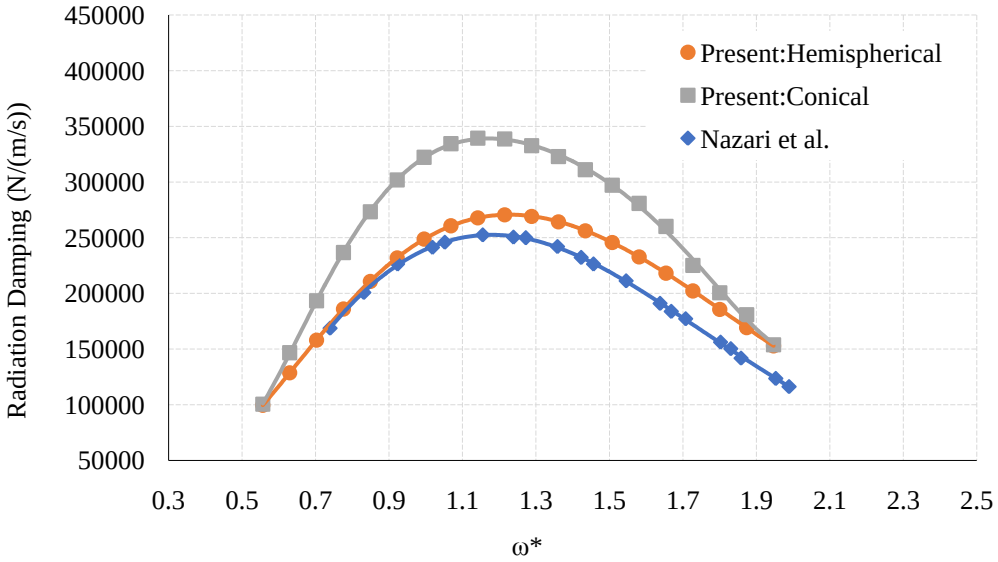

Figure 8. Comparison of radiation damping

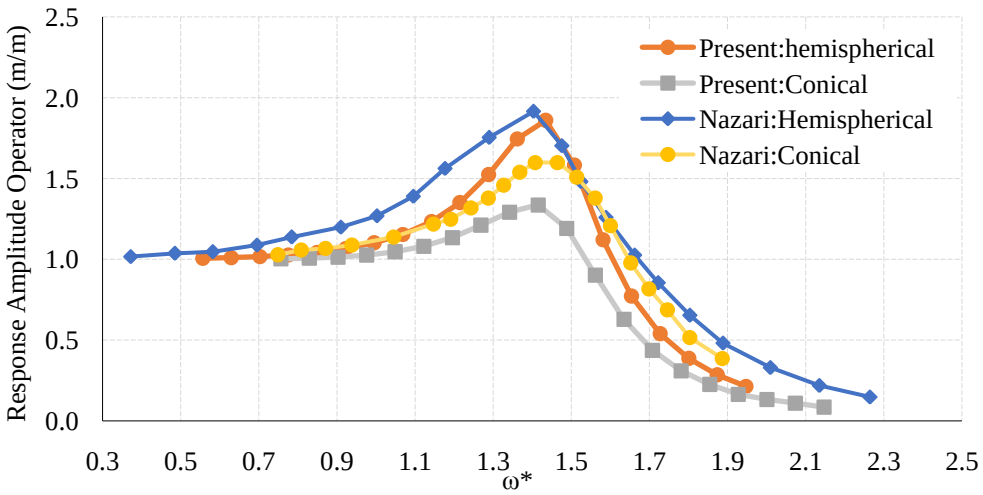

Figure 9. Comparison of heave RAO

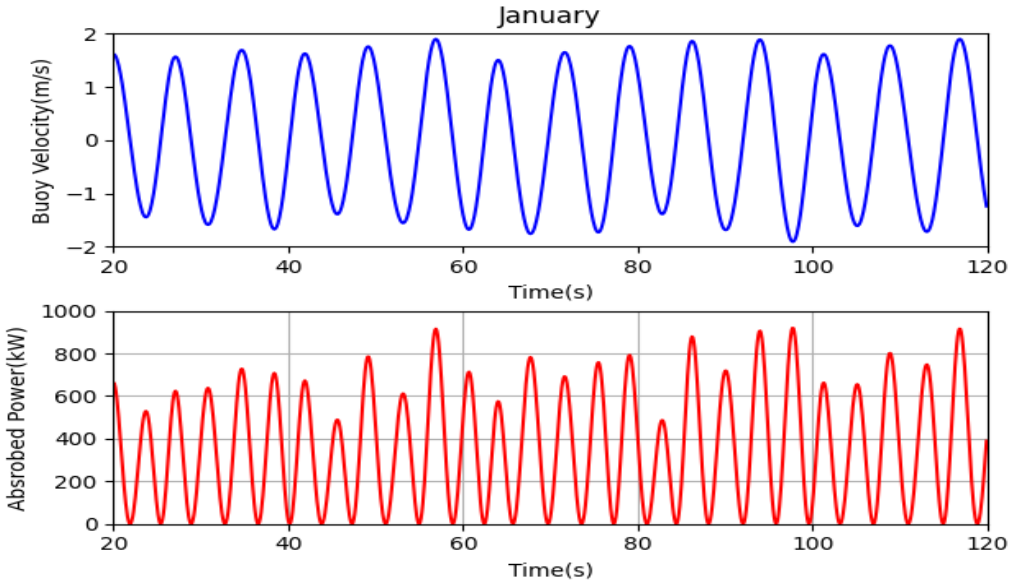

Figure 10. Time response analysis for a conical buoy in January 2012

The time response analysis was carried out from January to December, capturing the response of the buoy throughout the year. During this analysis, the variations in velocities were recorded, providing valuable insights into the dynamic behavior of the system in different wave conditions. As an example, the buoy velocity and the absorbed power of the conical buoy in January 2012 are presented in Figure 10. The average absorbed power is around 360 kW.

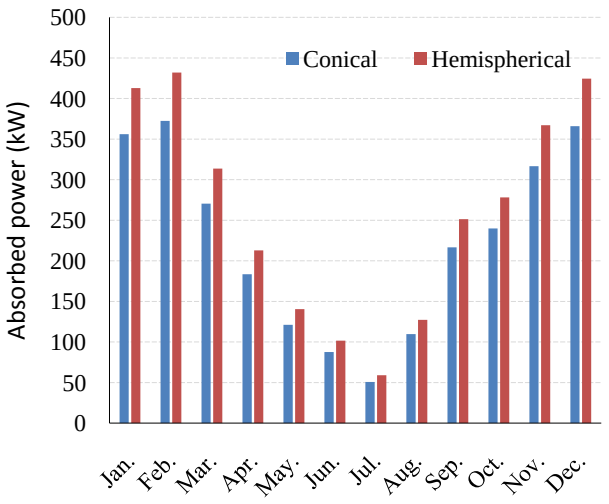

Figure 11. Mean monthly absorbed power (kW) (2012)

Figure 11 presents the mean monthly absorbed power in the Chengshantou area. The plot reveals that the absorbed power varies between 50 kW and 430 kW. Notably, higher power values are observed during the winter months, while lower power values are observed during the summer months. This suggests that the wave energy resource is more abundant and the buoy is capable of extracting more power during the winter season when the waves are larger and more energetic. On the other hand, the summer months experience lower wave energy, resulting in reduced power absorption.

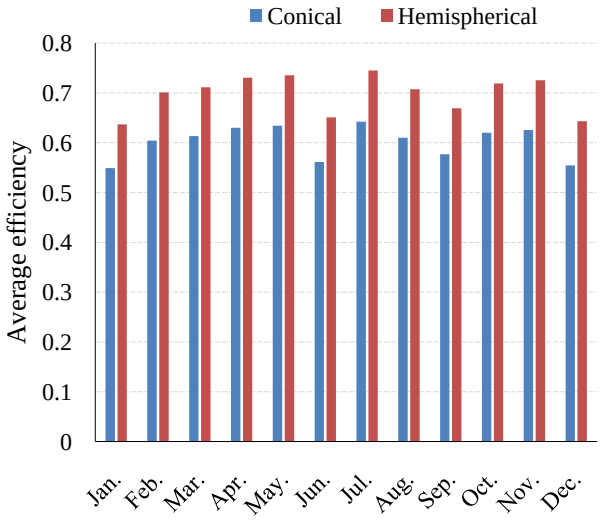

Figure 12. Average efficiency against each month (2012)

Figure 12 displays the mean monthly efficiency of two types of buoys: the hemispherical buoy and the conical buoy. The plot demonstrates that the mean monthly efficiency for the hemispherical buoy fluctuates around 0.7, while the conical buoy's efficiency fluctuates around 0.6. This indicates that the hemispherical buoy tends to exhibit a slightly higher efficiency in converting the available wave energy into usable power compared to the conical buoy. These efficiency values provide insights into the performance of the buoys under different wave conditions and aid in assessing their effectiveness for wave energy conversion.

4. Conclusions

The numerical simulations comparing the power extraction of the hemispherical and conical buoys have provided valuable insights. The following conclusion can be drawn:

- The hemispherical buoy, with better hydrodynamic characteristics, exhibits higher efficiency compared to the conical buoy. This implies that the interaction between the hemispherical buoy and the incident waves is smoother, allowing for more effective power absorption.
- The power absorption of the PAWEC is lowest during the summer months and highest during winter. This is consistent with the natural variations in wave energy, as summer typically experiences lower wave conditions compared to the more energetic winter waves.
- In terms of monthly power absorption, the minimum values are observed in July, with 58.9 kW for the hemispherical buoy and 50.8 kW for the conical buoy. On the other hand, the maximum power absorption occurs in February, with 431.8 kW for the hemispherical buoy and 372.2 kW for the conical buoy.
- The PAWEC operates with higher efficiency when operated near its natural frequency. The minimum efficiency is observed in January, with 63.7% for the hemispherical buoy and 54.9% for the conical buoy. Conversely, the maximum efficiency is observed in July, with 74.5% for the hemispherical buoy and 64.2% for the conical buoy.

Nomenclatures

J	energy density per unit width
P_{max}	maximum wave power
L_{max}	maximum absorption width
ρ	density of water
g	gravitational acceleration
T_e	wave period
H_s	significant wave height
M	displacement or mass of buoy
λ	wavelength
$\eta(t)$	wave profile
A	wave amplitude
α_{ij}	added mass matrix
β_{ij}	damping matrix
γ_{ij}	hydrostatic stiffness matrix
F_i	external force
M_{ij}	mass or mass moment of inertia of buoy
H	wave height
k	wave number
ω	wave frequency
M_a	added mass
C	radiation damping coefficient
F_e	excitation force
A_w	waterplane area
F_{hs}	hydrostatic force
F_d	diffraction force
F_{FK}	Froude-Krylov force
x_j	displacement matrix
$\dot{x}_j$	velocity matrix
$\ddot{x}_j$	acceleration matrix
P_{PTO}	absorbed power
δ_{PTO}	damping coefficient
Z	heave displacement

References

[1] A. Saket, A. "Etemad-Shahidi Wave energy potential along the northern coasts of the Gulf of Oman". Renew Energy 2012(40): 7-90.

[2] G. Iglesias, M. López, R. Carballo, A. Castro, JA Fraguela, P. Frigaard, "Wave energy potential in Galicia". Renew Energy 2009(34): 23-33.

[3] AFdO. Falcão "Wave energy utilization: a review of the technologies". Renew Sust Energy Rev 2010(14): 899-918.

[4] G. Iglesias, R. Carballo, "Wave energy and nearshore hot spots: the case of the SE Bay of Biscay". Renew Energy 2010(35): 249-500.

[5] H.R. Ghafari, H. Ghassemi, G. He. "Numerical study of the Wavestar wave energy converter with multi-point-absorber around Deep Cwind semisubmersible floating platform". Ocean Engineering 232, 1091772021.

[6] H.R. Ghafari, A. Neisi, H. Ghassemi, M. Iranmanesh. "Power production of the hybrid Wavestar point absorber mounted around the Hywind spar platform and its dynamic response". Journal of Renewable and Sustainable Energy 13 (3), 0333082021.

[7] E. Homayoun, H. Ghassemi, H. Ghafari. "Power performance of the combined monopile wind turbine and floating buoy with heave-type wave energy converter". Polish Maritime Research 26 (3), 107-1142019.

[8] E. Homayoun, S. Panahi, H. Ghassemi, G. He, P. Liu. "Power absorption of combined wind turbine and wave energy converter mounted on braceless floating platform". Ocean Engineering 266, 1130272022.

[9] S. Jahangiri, H. Ghassemi, HR. Ghafari, P. Ghadimi. "Power matrix of spherical and conical wavestar geometry with linear and circular arrangement". International Journal of Marine Engineering Innovation and Research, Vol. 7(3), Sept. 2022. 180-186.

[10] Y.L. Zhang, Z. Lin, Q.L. Liu. "Marine renewable energy in China: Current status and perspectives". Water Science and Engineering, 2014(7): 295-296.

[11] Gunn K, Clym S W. Quantifying the Global Wave Power Resource Renewable Energy 44 pp 296-304.

[12] P. Kumar, D. Singh, A. Ranjan Pau, A. Samad. "Design of a point absorber wave energy converter for an Indian coast". Journal of Physics: Conference Series, 2022(2217): 2-3.

[13] Bret Bosma, Zhe Zhang, Ted K.A. Brekken, H. Tuba Ö zkan-Haller, Cameron McNatt, Solomon C. Yim. "Wave Energy Converter Modeling in the Frequency Domain: A Design Guide". Energy, 2012: 2099-2102.

[14] M. Shadman, S F Estefen, C.A.Rodriguez, L.C.M. Nogueira, "A geometrical optimization method applied to a heaving point absorber wave energy converter". Renewable Energy, 2017(115): 46-533.

[15] C. J. Cargo, A. R. Plummer, A. J. Hillis and M. Schlotter "Determination of optimal parameters for a hydraulic power take-off unit of a wave energy converter in regular waves", Proceedings of the Institution of Mechanical Engineers Part A: Journal of Power and Energy, 2011, 226 (1) pp 98-111.

[16] J. Falnes, P.M. Lillebekken, "Budal's latching-controlled-buoy type wave-power plant". Proc. Fifth Eur. Wave Energy Conf. 2003, pp 233-44.

[17] B. Liang, F. Fan, Z. Yin, H. Shi, D. Lee. "Numerical modelling of the nearshore wave energy resources of Shandong peninsula, China". Renewable Energy 2013(57): 331-332.

[18] M. Nazari Berenjkoob, M. Ghiasi, C. Guedes Soares. "Influence of the shape of a buoy on the efficiency of its dual-motion wave energy conversion. Energy", 2021(214), 118998.